Supramolecular Structure and Function 8
(ed.: Greta Pifat-Mrzljak), Kluwer, New York,
2004, pp. 157–177.

Multi-Frequency EPR Spectroscopy Studies of the Structure and Conformational Changes of Site-Directed Spin Labelled Membrane Proteins

HEINZ-JÜRGEN STEINHOFF
Department of Physics, University of Osnabrück, Barbarastrasse 7, 49069 Osnabrück, Germany

1. INTRODUCTION

Electron paramagnetic resonance (EPR) spectroscopy of site-directed spin labelled biomolecules (site-directed spin labelling, SDSL) has emerged as a powerful method for studying the structure and conformational dynamics of proteins and nucleic acids under conditions relevant to function[1-5]. In this technique, a spin label side chain is introduced at a selected site via cysteine substitution mutagenesis followed by modification of the unique sulfhydryl group with a specific paramagnetic nitroxide reagent (Fig. 1). The continuous wave (cw) EPR spectrum yields information about the nitroxide side chain mobility, the solvent accessibility, the polarity of its immediate environment and the distance between the nitroxide and another paramagnetic centre in the protein. EPR data analysis of a series of spin labelled variants of a given protein allows definition of elements of secondary structure, including their solvent exposure, to characterize protein topography and to determine orientations of individual segments of the protein. A complete analysis allows modelling of protein structures with a spatial resolution at the level of the backbone fold[2, 3, 6-9]. The method is applicable to any protein that retains its function after spin labelling. One of the most powerful properties of the method is its sensitivity to molecular dynamics: protein equilibrium fluctuations and conformational

changes of functional relevance can be followed on a wide time scale ranging from picoseconds to seconds. The present report presents applications of this method to a selected set of membrane proteins: The light driven proton pump bacteriorhodopsin (BR) (cf. Fig. 2a) and the sensory rhodopsin – transducer complex, pSRII-pHtrII, responsible for phototaxis may be regarded as model systems for ion pumps and signal receptors. The Na^+/proline transporter PutP is a model for the Na^+/substrate symporter family (SSSF) which currently comprises more than 200 similar proteins of pro- and eukaryotic origin[10]. Investigation of the structure and conformational dynamics of these classes of membrane proteins represents one of the current major challenges.

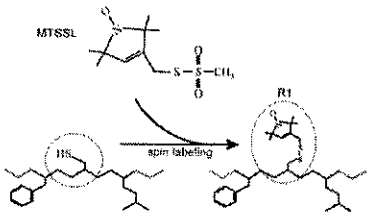

Figure 1. The reaction of the methanethio-sulfonate spin label (MTSSL)[11] with a sulfhydryl group generates the spin label side chain R1.

2. SPIN LABEL DYNAMICS AND SOLVENT ACCESSIBILITY

The relationship between the nitroxide side chain mobility and the protein secondary and tertiary structure has been extensively reviewed[12-16]. The term "mobility" is used here in a general sense and includes effects due to the motional rate, amplitude and anisotropy of the nitroxide reorientation. Weak interaction between the nitroxide and neighbouring side chain or backbone atoms as found for helix surface sites or loop regions results in a high degree of mobility. In this case the apparent hyperfine splitting and the line width are small. In turn, strong interaction of the nitroxide group with adjacent side chain or backbone atoms restricts its reorientational motion. Hence, tertiary contact or buried sites are characterized by an increased apparent hyperfine splitting and line width. Figure 2b shows an example of

three spin labelled sites of bacteriorhodopsin. Two sites, positions 163 and 164, are located in the loop connecting helices E and F. The spin label side chain at position 164 is oriented to the aqueous phase. Nearly unhindered reorientational motion of the nitroxide is possible within a large motion cone as revealed by molecular dynamics simulations[17]. This motion leads to considerable averaging of the anisotropic contribution of the hyperfine interaction. Hence, the apparent hyperfine splitting is expected to be small in agreement with the experimental result. The side chain at position 163 is oriented away from the aqueous phase into the direction of helices B and C. The reorientational motion of the nitroxide is more restricted. Consequently, averaging of the anisotropic hyperfine interaction is less complete. The nitroxide at position 170 is buried within the protein. The nitroxide motion is completely restricted and the EPR spectrum resembles that of a nitroxide powder spectrum. Depending on the length and flexibility of the linker between the nitroxide and the protein backbone and possible hydrogen bonding of the nitroxide to the protein the flexibility of the protein backbone itself contributes to the overall nitroxide mobility. Numerous examples have shown that the analysis of the nitroxide dynamics of a series of spin labelled protein variants uncovers the secondary structure and provides important information about tertiary interaction[2, 16, 18, 19].

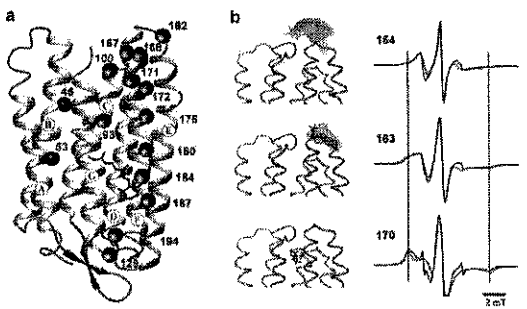

Figure 2. (a) Structure of bacteriorhodopsin. A selection of the spin labelled positions discussed in this text is highlighted. *(b)* Motional freedom of the spin label side chains at different positions in the E-F loop and in helix F of bacteriorhodopsin. The dotted area represents the accessible space of the nitroxide covered within a high temperature (600K) molecular dynamics simulation of 6 ns length[17]. The different degree of mobility of the nitroxides is reflected in the variation of the apparent hyperfine splitting of the corresponding experimental spectra (T = 293K) (continuous line) and the spectra calculated on the basis of the molecular dynamics trajectories (dotted).

The collision frequency of the nitroxide side chains with freely diffusing paramagnetic probe molecules provides additional structural information. The collision frequency of such a probe depends on the product of its translational diffusion coefficient and its local concentration. Molecular oxygen and water soluble paramagnetic Ni(II) complexes or chromium oxalate have been frequently used and are ideally suited because of their sizes and solubility properties[20-22]. In a water/membrane system these molecules are partitioned between the water and the hydrophobic phase according to their polarity. Polar metal complexes preferentially partition into the aqueous phase, whereas apolar oxygen exhibits a maximum value of the product of concentration and diffusion coefficient in the centre of the membrane bilayer[23]. The determination of the collision frequency of nitroxide side chains with these paramagnetic reagents in solution allows identification of the side chain orientations with respect to the protein-water or protein-lipid interface. Continuous wave power saturation has been shown to provide an easy and reliable means for the quantification of the collision frequencies[23].

3. POLARITY OF THE SPIN LABEL MICRO-ENVIRONMENT

The application of high-field EPR techniques with Lamor frequencies exceeding 90 GHz has considerably enhanced the Zeeman resolution of rigid-limit spectra of disordered spin labelled samples. The principal g-tensor components and their modulation due to solute-solvent interactions can be determined with high accuracy[24-26]. The structural information is contained in the variation of the polarity in the spin label micro-environment. A polar environment shifts the tensor component g_{xx} of a nitroxide to smaller values whereas the hyperfine tensor component A_{zz} is increased[27, 28] (cf. Fig.3). Hence, both tensor components can be regarded as polarity indexes. In addition, a plot of g_{xx} *vs.* A_{zz} allows discrimination between protic and aprotic environment due to the different sensitivities of these tensor components towards the influence of hydrogen bonding to the NO group[28, 29]. In a sequence of a regular secondary structure with anisotropic solvation, the local water density in the vicinity of the spin labelled site and hence the polarity index values are a periodic function of sequence number, similar to the behaviour of the nitroxide mobility or its accessibility for water soluble paramagnetic ions.

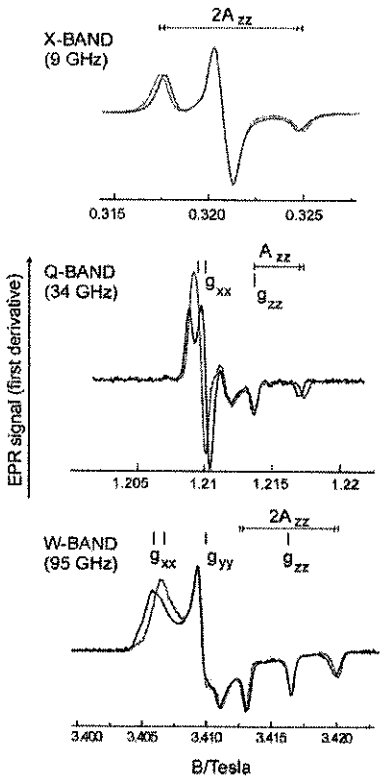

Figure 3. EPR spectra of MTS spin label in micro-environments of low (continuous line) and high (dotted line) polarity: *(top),* X-band spectra of bacteriorhodopsin variants L93R1 (protein interior, continuous line) and K129R1 (extracellular surface, dotted line)[30]; *(middle),* Q-band spectra of the spin label in frozen polystyrene/toluene (continuous line) and ethanol/water mixtures (dotted line); *(bottom),* W-band spectra of bacteriorhodopin variants T46R1 (protein interior, continuous line) and M163R1 (cytoplasmic surface, dotted line)[29].

3.1 Polarity profile along the bacteriorhodopsin proton channel

Sample spectra of spin label side chains attached along the bacteriorhodopsin proton channel are shown in figure 4. The variation of g_{xx} with the nitroxide binding site is revealed by the shift of the position of the low-field maximum. This shift is observable already in the Q-band (34 GHz) spectra (Reyher and Steinhoff, unpublished) and is clearly resolved in W-band (95 GHz) spectra[29]. Fittings of simulated powder spectra to the experimental data yielded the components of the g-tensor and of the hyperfine tensor with high accuracy (see Figs. 5 and 6). The plot of g_{xx} *vs.* nitroxide position along the proton channel reveals distinct variations in the polarity of the nitroxide micro-environment (Fig. 5a). The high polarity in the environment of residues at the cytoplasmic and extracellular surfaces, positions 162, 163, 166, 168 and 129, is clear evidence that these nitroxides are accessible to water, which is in agreement with the structure. The environmental polarity reaches its minimum close to position 46 between the proton donor D96 and the retinal, again in agreement with the protein structure. The g_{xx} behaviour provides quantitative information about the hydrophobic barrier the proton has to overcome on its way through the protein.

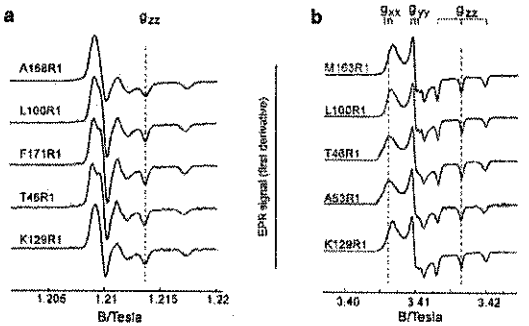

Figure 4. (a) Q-band (34 GHz) and *(b)* W-band (95GHz) EPR spectra[29] of spin labels introduced along the proton channel of bacteriorhodopsin (cf. Fig. 2a). The variation of the local polarity is revealed by the different shapes of the Q-band spectra at their low field resonance position (1.208 T) and by a clear shift of the respective resonance peak at the g_{xx}-position in the W-band spectra (3.46 T).

3.2 Polarity profile along the protein-lipid interface

The polarity variation along the lipid-exposed surface of transmembrane protein elements can be used to locate the spin labelled sites with respect to the lipid-water interface. These data provide information on the topology of membrane protein elements, their orientation with respect to the lipid phase[31] and possible water penetration along the protein-lipid interface. Experimental results for helix F of BR are shown in figure 5b. The component A_{zz} of the hyperfine tensor reveals polar micro-environments for sites 162 and 168 at the cytoplasmic surface of BR and at position 129 close to its extracellular surface. As discussed above, the nitroxides attached to these sites are accessible for water molecules in agreement with the protein structure. The minimum values for A_{zz} are found for the nitroxides at positions 180, 184 and 187. According to the BR structure these sites are oriented to the lipid phase and located close to the centre of the membrane (cf. Fig. 2a). The values of A_{zz} found for positions 172 and 176 are between these polar and non polar limits. The behaviour of this polarity profile along the transmembrane helix F of BR is in line with the polarity profile found in frozen protein free hydrated lipid bilayers[32]. Restricted water penetration along the protein lipid interface might be the explanation for the relatively high polarity values in the vicinity of positions 172 and 176.

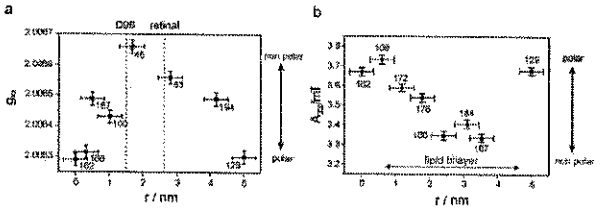

Figure 5. (a) The tensor element g_{xx} of spin labels oriented towards the aqueous phase or into the proton channel of BR as a function of the nitroxide location with respect to position 164[29]. The dotted lines indicate the positions of D96 and the Schiff-base of retinal, respectively. *(b)* The hyperfine tensor component A_{zz} for spin label side chains bound to the surface of helix F of BR as a function of the nitroxide location with respect to position 164[33] (Wegener, Pfeiffer, Steinhoff, unpublished). Here, the nitroxides are oriented either to the aqueous or to the lipid phase. The purple membrane spans the range from approximately 0.6 to 4.6 nm. The uncertainty of the nitroxide positions (horizontal error bars) was estimated from molecular modelling of different spin label side chain orientations with respect to the helix. Measurements were performed with frozen suspensions of purple membrane (170 K).

The analysis of g_{xx} as a function of the hyperfine tensor component A_{zz}, provides additional information on the proticity of the micro-environment of the spin label side chain. This dependence is plotted in Fig. 6 for the various spin label positions in BR. As pointed out earlier[29], the plot is suggestive of straight-line correlations. Theoretically, both g_{xx} and A_{zz} are expected to be linearly dependent on the π spin density ρ_O at the oxygen atom of the nitroxide group[28]. For A_{zz} this is evident from the relation $A_{zz} \propto \rho_N$ and the condition $\rho_N + \rho_O \approx 1$. For g_{xx}, however, apart from a direct proportionality to ρ_O, there is an additional dependence on specific electronic properties of the oxygen lone-pair orbitals, such as their degree of s, p_x, p_y –hybridization and their orbital energy. The lone-pair orbital energy E_n affects g_{xx} via the excitation energy $\Delta E_{n->\pi^*} = E_{\pi^*} - E_n$ and is known to be sensitive to a polar environment, e.g. water, and to be particularly sensitive to direct H-bonding of the lone pairs to water or to polar amino acid residues[28]. Deviations from the straight line connecting the data of the polar (ethanol/water) and apolar (polystyrene/toluene) limits in the direction of higher/lower g_{xx}-values may therefore indicate a more aprotic/protic micro-environment of the nitroxide[28].

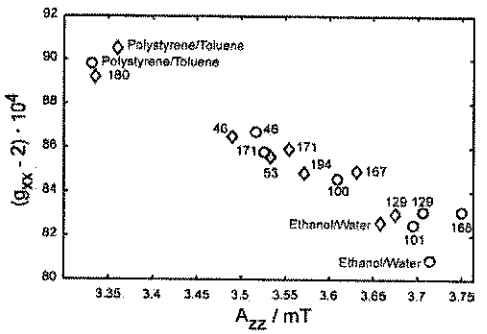

Figure 6. Plot of g_{xx} *vs.* A_{zz} of the nitroxide for various spin label positions in BR and for MTSSL in polystyrene/toluene or ethanol/water mixtures. Experimental errors for Q-band data (circles, Reyher and Steinhoff, unpublished) were estimated to be less than $\pm 5 \cdot 10^{-5}$ for g_{xx} and ±0.05 mT for A_{zz}. For W-band (diamonds) (data taken from Steinhoff et al.[29]) experimental errors are less than $\pm 2 \cdot 10^{-5}$ for g_{xx} and ±0.02mT for A_{zz}. Q-band and W-band data coincide within experimental error. The plot reveals that the polarity and proticity properties at the helix-lipid interface close to the centre of the purple membrane (position 180 in helix F of BR) resemble those of a polystyrene/toluene mixture.

4. INTER-SPIN DISTANCE MEASUREMENTS

The simultaneous exchange of two native amino acids by cysteines followed by modification with spin labels allows determination of inter-residual distances[34, 35] and thus provides a strategy for deducing proximity of selected secondary structural elements.

The spin-spin interaction between two spin labels attached to a protein is composed of static dipolar interaction, modulation of the dipolar interaction by the residual motion of the spin label side chains and exchange interaction. The static dipolar interaction leads to considerable broadening of the cw EPR spectrum if the inter-spin distance is less than 2 nm. For unique orientations of the nitroxides relative to each other as found for spin labels introduced at buried sites in the rigid limit a rigorous solution of the spin Hamiltonian of the system can be obtained. Spectra simulations yield the distance between the nitroxides and the Euler angles describing their relative orientation and that of the inter-spin vector relative to the magnetic field[34, 36]. For surface sites, the nitroxides may adopt a statistical distribution of distances and relative orientations. Values of the inter-spin distances can be determined from a detailed line shape analysis of spectra measured below 200 K[37-39] or in solutions of high viscosity[40] using spectra convolution or deconvolution techniques. Here, the superposition of the powder spectra of the two nitroxides is regarded as to be convoluted with the Pake pattern resulting from the dipolar interaction within the nitroxide pair. The nitroxides and the inter-spin vector are assumed to be randomly oriented in space. Since the spin labelling efficiency is less than 100% a variable fraction of singly spin labelled protein has to be accounted for. The lower limit for reliable distance determination using the above methods is given by the increasing influence of exchange interaction for inter-spin distances less than 0.8 nm due to partial overlap of the nitrogen pi-orbitals of the two interacting nitroxides.

The method of inter-spin distance determination has been successfully applied to a number of proteins, including rhodopsin[41, 42], lac permease[43], the KcsA potassium channel[8, 44] and alpha-crystallin[7]. In addition, changes in dipolar interaction can result in large spectral changes, making it straightforward to monitor conformational changes[44-46] (see below).

For inter-spin distances exceeding 2 nm the line broadening due to dipolar interaction is much less than the influence of other homogeneous and inhomogeneous contributions. Here pulsed EPR techniques are much more powerful. These techniques include pulsed ELDOR techniques such as four-pulse double electron-electron resonance (DEER)[47], the 2 + 1 pulse sequence[48], multiple-quantum EPR[49], and single-frequency techniques for refocusing (SIFTER) electron-electron couplings[50, 51].

Metal ion - nitroxide interactions in metallo-proteins or engineered copper-ion-binding sites allow estimation of intramolecular distances also at room temperature[52, 53]. A single metal ion provides a reference site for the estimation of distances to multiple nitroxide sites[54].

One attractive feature of site directed spin labelling is the ability to time resolve changes in any of the parameters discussed above. Changes in the protein secondary structure, protein tertiary fold or domain movements can be followed with up to 0.1 ms resolution with conventional EPR instrumentation and detection schemes (field modulation). Important examples found in the literature include the detection of rigid body helix motion in both rhodopsin and bacteriorhodopsin[45, 55-58], domain movements in T4 lysozyme[1], structural reorganization in colicin E1[59] upon membrane binding and conformational changes during signal transfer from sensory rhodopsin pSRII to the transducer pHtrII [9].

4.1 Inter-spin distances and distance changes in spin labelled bacteriorhodopsin

As an example for the elucidation of protein structure and conformational dynamics using dipole-dipole interaction within doubly spin labelled protein variants, an application of the method to BR is described. After light excitation BR undergoes a catalytic cycle, the so called photocycle, during which a proton is pumped from the cytoplasmic to the extracellular side of the membrane. The proton transport is accompanied by conformational changes as revealed by several different biophysical techniques (for a summary see, e.g., Subramaniam et al.[60, 61]). EPR spectroscopy of spin labelled BR mutants uncovered the time course of this conformational change[56-58, 62, 63]. Transient alterations of the spin label mobility during the BR photocycle were found in the loop regions A-B, C-D and E-F on the cytoplasmic surface of the protein. The results indicated a transient outward movement of the cytoplasmic part of helix F during the so called M intermediate of the photocycle which is characterized by a deprotonated Schiff base.

For a quantitative analysis of the structural changes pairs of spin labels were introduced into the C-D loop and the E-F loop. Five of these spin labelled positions are indicated in figure 7d. Corresponding EPR spectra of doubly spin labelled BR mutants are depicted in figure 7a and 7b. X-band[63] and Q-band spectra (A. Holt, Bachelor thesis, unpublished) of doubly spin labelled BR mutants are compared to the superposition of the spectra of the corresponding singly spin labelled samples. The doubly labelled samples show broader lines and consequently smaller amplitude due to spin-spin

interaction. This increase of the line width is especially pronounced in the rising edge of the low field region of the Q-band spectra. Fitting of simulated powder spectra to the experimental data yielded inter-spin distance values and the fraction of singly labelled protein in the samples[63]. The values determined from X- and Q- band spectra for each double mutant agree within experimental error (A. Holt, Bachelor thesis, unpublished). A comparison of these values with inter-nitroxide distances determined from molecular dynamics simulations of the spin labelled protein reveals also nice agreement. Hence, the structure of the cytoplasmic moieties of helices C, E and F in the native purple membrane environment resembles that of the crystal structure. The fitting uncovered an amount of between 40% and 50% of non-interacting nitroxides. This percentage is in agreement with the experimentally determined spin labelling efficiency of between 70% and 80%.

Inter-spin distance changes during the photocycle were detected by freezing BR in different intermediates. The intermediate showing the largest conformational change was stabilized by illuminating the sample at 230 K with $\lambda > 580$ nm and fast cooling to 170 K in the dark. FT-Raman spectroscopy showed that this protocol lead to accumulation of the M intermediate to approximately 75%[63]. Compared to the ground state spectrum the line width of the M intermediate state spectrum of V101R1&A168R1 is considerably reduced. The inter-spin distance was calculated from the experimental data to increase by at least 0.1 nm. Concurrently, the dipolar line broadening visible in the EPR spectra of L100R1&S226R1 increased (data not shown). The corresponding inter-spin distance decrease amounts to 0.2 nm. No changes of the inter-spin distances were detected for V101R1&A160R1. These results reveal an outward movement of the cytoplasmic end of helix F and an inward tilt of helix G into the direction of the proton channel as shown in figure 7d. There is no distance change detectable between the positions 101 and 160, hence helices C and E are most probably not affected in the observed conformational change.

The time course of the helix movements in BR was resolved at room temperature by detection of the EPR signal amplitude changes at fixed B-field positions. This is again exemplified for the double mutant V101R1&A168R1 which monitors the outward movement of helix F (figure 7c).

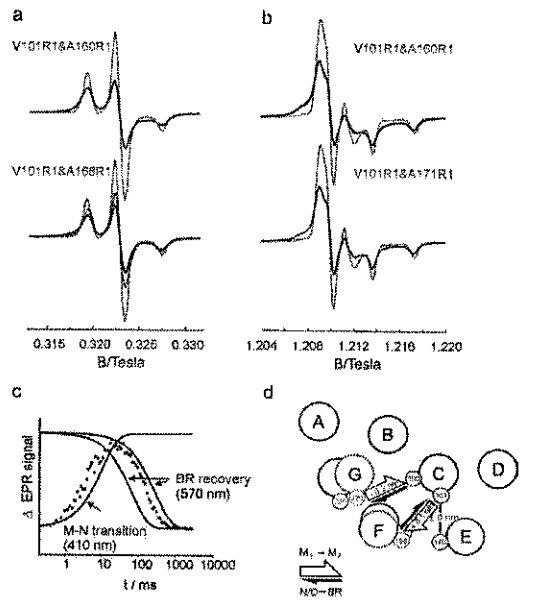

Figure 7. Low temperature (170 K) EPR spectra of BR double mutants V101R1&A160R1, V101R1&A168R1 and V101R1&A171R1 determined at *(a)* X-band[63] and *(b)* Q-band (A. Holt, Bachelor thesis, unpublished). Pronounced dipolar broadening is observed for the initial state (continuous lines) as revealed by the comparison with the superposition of the spectra of the singly labelled mutants (dotted lines). Illumination at 220 K and fast cooling to 170 K decreased the line width for the doubly labelled mutant (V101R1&A168R1, dashed line). All spectra are normalized to a constant spin number. *(c)*, EPR signal changes of the centre line of sample V101R1&A168R1 after photo-excitation[63] (squares, X-band, T=293 K). The solid lines show the time course of the M to N transition and two dominating rates of the recovery of the BR initial state determined by a multi-exponential fit of transients determined at 410 and 570 nm, respectively. The inter-spin distance between positions 101 and 168 increases prior to the M decay and returns into its initial value with a time course that can be fitted with the two dominating time constants of the BR initial state recovery. *(d)*, Top view of the cytoplasmic surface of BR with indicated inter-spin distances for the BR initial state and distance changes occurring during the photocycle. According to the EPR inter-spin distance measurements the outward movement of the cytoplasmic terminus of helix F by 0.1 nm is accompanied by an inward shift of the cytoplasmic terminus of helix G by 0.2 nm[63].

After light activation a transient increase of the amplitude of the centre line due to a transient decrease of the dipolar interaction was observed. Time constants of the rise and decay of the transient EPR signal were determined from fitting of a superposition of exponentials. A comparison with the respective time constants for the photocycle intermediates of BR determined from optical and FTIR spectroscopy revealed that the observed conformational change occurs in phase or slightly prior to the decay of the M intermediate[63]. Hence, the trigger for this conformational change must be independent from the reprotonation of the Schiff base. The recovery of the ground state conformation of helix F can be satisfactorily fitted with the two dominating relaxation time constants of the optical transient determined at 570 nm which indicates the back reaction of the retinal to its initial state.

4.2 Protein-protein interaction: the sensory rhodopsin – transducer complex

The archeabacterial photoreceptors sensory rhodopsin I (SRI) and II (SRII) provide the initial signal which enables the cells to seek favourable light conditions (for reviews, see, e.g., Spudich et al.[64, 65]). The two photoreceptors are tightly complexed to receptor specific transducers (HtrI and HtrII). A light induced signal is transferred from the receptor to the cytoplasmic domain of the transducer which activates a two-component signalling cascade well known from bacterial chemotaxis. Both transducers contain two membrane spanning helices which are thought to be involved in the signal transfer.

A structural model of the pSRII - pHtrII complex from *Natronobacterium pharaonis* was determined from an EPR analysis of a set of singly and doubly spin labelled protein variants reconstituted into purple membrane lipid bilayers (Fig. 8)[9]. Inter-spin distances were obtained for 26 pairs of spin labels introduced into the transmembrane helices TM1 or TM2 of the transducer pHtrII and helices F or G of the receptor pSRII. Considerable spin-spin interactions observed for the singly labelled transducer with the nitroxide side chain located at positions 78 or 82 confirmed a dimeric arrangement of TM2 and TM2'. The strongest interaction corresponding to the closest distances (less than 1.2 nm) between pSRII and pHtrII were observed between positions 25 and 210, 81 and 210, and between 81 and 211 indicating that both TM1 and TM2 are close to helix G. According to these inter-spin distance values and the distances between the other pairs TM2 had to be located between the C-terminal helices F and G as depicted in figure 8[9]. The results revealed a quaternary complex between two copies of pHtrII

and pSRII each, forming a structure with an apparent two-fold symmetry. The crystal structure of the complex confirmed the EPR derived model[66].

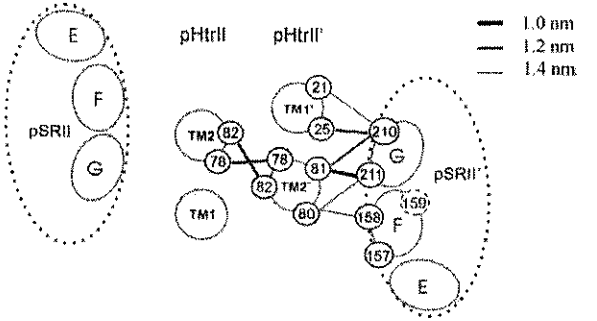

Figure 8. Schematic model of the transmembrane region of the 2:2-complex of pSRII with its transducer pHtrII (view from the cytoplasm). The transmembrane helices of the transducer, TM1 and TM2, and helices E, F and G of the receptor were oriented with respect to each other based on dipolar spin-spin interactions and derived distance constraints[9]. Strong dipolar interactions due to inter-spin distances less than 1.4 nm between spin labelled positions of pSRII and pHtrII or within the pHtrII dimer are coded by the thickness of connecting lines.

On light excitation the pSRII receptor reverts to the long lived M-intermediate which was proposed to represent the signalling state[67]. During this reaction helix F of the receptor moves outwardly similar to the conformational change found in BR[68] (see also Fig. 7d). This helix movement of the receptor is transferred to the transducer as revealed by comparing the inter-residual distance changes observed between transducer / transducer as well as receptor / transducer[9]. Low temperature experiments (T = 170 K) with the receptor trapped in the M intermediate showed decreases and increases of the interaction strengths between the TM2 and TM2' and between TM2 and helix F of pSRII. Residues S158R1 and K157R1 of helix F approached TM2-residues A80R1 and T81R1 in M. Concurrently, the strong dipolar interaction between the two V78R1 in neighbouring TM2 helices was significantly reduced revealing a rearrangement of TM2.

In figure 9 the time course of the EPR signal change of V78R1 at fixed B-field position is compared to that of L159R1. The nitroxides at positions V78R1 of TM2 and V78R1' of TM2' face each other leading to considerable dipolar broadening of the spectra. L159R1 is located in helix F and oriented

towards the inside of the receptor (cf. figure 8). An optical trace monitoring the depletion and reformation of the pSRII ground state (measured at 500 nm) is also depicted in figure 9. The kinetic EPR difference spectra recorded at room temperature represented features of a transient increase of the inter-spin distance for sample V78R1 and a transient mobilization for L159R1[9]. Thus, the three signals shown in figure 9 record events occurring at the level of the retinal chromophore (500 nm optical trace), of helix F (L159R1, EPR trace), and of TM2 (V78R1, EPR trace) which allows to follow the signal transfer in the sequence retinal - helix F - TM2 and vice versa. After absorption of a photon by the retinal the activated state remains unchanged for about 100 ms. With the reformation of the ground state, the reaction of the receptor seems to be decoupled from that of the transducer. The movement of helix F into the original position seems to precede the recovery of TM2 position. This decoupling allows the system to modulate the activation/deactivation of the transducer, thereby enabling the bacteria to respond to external stimuli adequately[9].

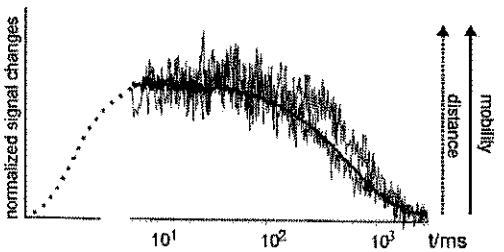

Figure 9. EPR transients (noisy lines) and the corresponding optical traces recorded at 500 nm (continuous line) of the receptor – transducer complex pSRII - pHtrV78R1 (dotted line), and of L159R1-pHtrII (continuous line) after light activation (T=293K)[9]. The EPR signal changes in the complex uncover a transient increase of the distance between positions 78 and 78' of the two transmembrane helices of the transducer dimer, TM2 and TM2' (see Fig. 8). The transient increase of the mobility of the spin label side chain L159R1 indicates an outward movement of helix F of pSRII[9] similar to that found in BR[61]. The rise of the EPR signals could not be resolved in this experiment.

4.3 Inter-spin distance determination by four-pulse DEER in PutP

Double electron-electron resonance (DEER)[47], in combination with site-directed spin labelling, has been applied to determine details of the so far unknown structure of the Na^+/proline transporter PutP of Escherichia coli[69]. PutP is a member of the Na^+/substrate symporter family (SSSF) which currently comprises more than 200 similar proteins of pro- and eukaryotic origin[10]. These integral membrane proteins utilize the Na^+ electrochemical gradient to drive the transport of a variety of substrates like, e.g., sugars, amino acids and vitamins. Biochemical and biophysical studies suggest a secondary structure model according to which PutP contains 13 transmembrane helices (TMs) with the N terminus located on the periplasmic side of the membrane and the C terminus facing the cytoplasm[70, 71] (see also figure 10).

EPR spectroscopy data of singly spin labeled PutP variants[71] in the presence and absence of Na^+ or proline lead to the conclusion that binding of ligands induces conformational alterations that involve at least part of TM II and the preceding cytoplasmic loop (loop L2). Further investigations of the arrangement of the cytoplasmic loops were performed with the double cysteine PutP derivatives L37C&A107C and L37C&D187C. These variants were used to determine distances between the cytoplasmic loops L2 and L4 and between the loops L2 and L6. In addition the doubly spin labeled PutP derivative A107C&S223C provide nitroxides positions on different sides of the lipid membrane (loops L4 and L7).

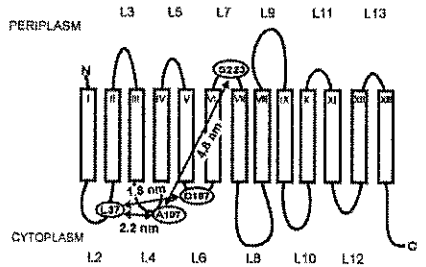

Figure 10. Secondary structure model of PutP with the spin labelled sites highlighted. Given are the mean distances between these sites as determined by four-pulse DEER[69].

Cw EPR experiments showed that the inter-spin distances within these three samples exceed 1.8 nm. Hence, DEER experiments were performed which were shown to provide inter-spin distance resolution in the range from 2 to 8 nm[72]. By using a model-free direct transformation of the DEER time domain data with the crosstalk-corrected approximate Pake transformation (APT)[73] a broad distance distribution was obtained for the doubly spin labeled mutant L37R1&D187R1 (Fig. 11). The maximum of the distribution was found to be close to the lower distance limit of the pulse DEER method (~1.8 nm) and the asymmetric width of the distribution was estimated to approach 0.8 nm. The results suggest that the loops L2 and L6 are in close proximity and that these regions are very poorly ordered. Although L37 itself is not important for PutP function, R40 in its vicinity plays an important role in coupling of Na^+ and proline transport[74]. Similarly, D187 in loop L6 is crucial for an efficient coupling of the transport of both ligands[75]. Both residues are highly conserved within the SSSF. The DEER measurements provided evidence that R40 and D187 may interact with each other during the transport cycle. This is even more pronounced by the observation that the distance between positions 37 and 187 increased upon Na^+ binding (cf. Fig. 11). In contrast to that, Na^+ and proline did not significantly influence the DEER signal of L37R1&A107R1. This indicates that the relative arrangement of loops L2 and L4 are only minor modulated by the ligands. The large value of 4.8 nm for the inter-spin distance determined between position 107 in loop 4 and position 223 in loop 7 is strong evidence that these positions are located on opposite sides of the membrane. The above results demonstrate that four-pulse DEER spectroscopy is a powerful means to investigate the structure and conformational changes of integral membrane proteins reconstituted in liposomes.

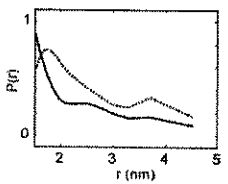

Figure 11. Inter-spin distance distribution, P(r), for spin label side chains L37R1 and D187R1 in the absence (continuous line) and presence of Na^+ (dotted line) as determined by pulse DEER (modified[60]). The shift of the maximum of P(r) reveals that loops L2 and/or L4 of PutP undergo a Na^+ induced conformational change.

ACKNOWLEDGEMENTS

We gratefully acknowledge the support of the Deutsche Forschungsgemeinschaft (SFB431-P18).

REFERENCES

1. Hubbell, W.L., H.S. McHaourab, C. Altenbach, and M.A. Lietzow, 1996, Watching proteins move using site-directed spin labeling. *Structure* 4: 779-783.
2. Hubbell, W.L., A. Gross, R. Langen, and M.A. Lietzow, 1998, Recent advances in site-directed spin labeling of proteins. *Curr. Opin. Struct. Biol.* 8: 649-656.
3. Hubbell, W.L., D.S. Cafiso, and C. Altenbach, 2000, Identifying conformational changes with site-directed spin labeling. *Nat. Struct. Biol.* 7: 735-739.
4. Feix, J.B. and C.S. Klug, Site-directed spin labeling of membrane proteins and peptide-membrane interactions, in *Spin Labeling: The Next Millenium*, L.J. Berliner, Editor. 1998, Plenum Press: New York. p. 251-281.
5. Steinhoff, H.-J., 2002, Methods for study of protein dynamics and protein-protein interaction in protein-ubiquitination by electron paramagnetic resonance spectroscopy. *Frontiers in Bioscience* 7: c97-110.
6. Mchaourab, H.S. and E. Perozo, Determination of protein folds and conformational dynamics using spin-labeling EPR spectroscopy., in *Distance Measurements in Biological Systems by EPR*, L.J. Berliner, Eaton, S.S., Eaton, G.R., Editor. 2000, Kluwer: New York.
7. Koteiche, H.A. and H.S. Mchaourab, 1999, Folding pattern of the a-crystallin domain in aA-crystallin determined by site-directed spin labeling. *J. Mol. Biol.* 294: 561-77.
8. Perozo, E., D.M. Cortes, and L.G. Cuello, 1998, Three-dimensional architecture of a K+ channel: implications for the mechanism of ion channel gating. *Nature of Structural Biology* 5: 459-469.
9. Wegener, A.A., J.P. Klare, M. Engelhard, and H.-J. Steinhoff, 2001, Structural insights into the early steps of receptor-transducer signal transfer in archaeal phototaxis. *EMBO J.* 20: 5312-5319.
10. Jung, H., 2001, Towards the molecular mechanism of Na+/solute symport in prokaryotes. *Biochim. Biophys. Acta* 1505: 131-143.
11. Berliner, L.J., J. Grunwald, H.O. Hankovszky, and K. Hideg, 1982, A novel reversible thiol-specific spin label: papain active site labeling and inhibition. *Anal. Biochem.* 119: 450-455.
12. Berliner, L.J., *Spin Labeling : Theory and Applications*. 1976, New York: Academic Press.
13. Berliner, L.J., *Spin Labeling II: Theory and Applications*. 1979, New York: Academic Press.
14. Berliner, L.J. and J. Reuben, *Biological Magnetic Resonance. Vol. VIII: Spin Labeling Theory and Applications*, ed. L.J. Berliner and J. Reuben. 1989, New York: Plenum Press.
15. Berliner, L.J., *Spin Labeling: The Next Millenium*. 1998, New York: Academic Press.

16. Mchaourab, H.S., M.A. Lietzow, K. Hideg, and W.L. Hubbell, 1996, Motion of spin-labeled side chains in T4 lysozyme. Correlation with protein structure and dynamics. *Biochemistry* **35**: 7692-704.
17. Steinhoff, H.J., M. Müller, C. Beier, and M. Pfeiffer, 2000, Molecular dynamics simulation and EPR spectroscopy of nitroxide side chains in bacteriorhodopsin. *J. Molecular Liquids* **84**: 17-27.
18. Pfeiffer, M., T. Rink, K. Gerwert, D. Oesterhelt, and H.J. Steinhoff, 1999, Site-directed spin-labeling reveals the orientation of the amino acid side-chains in the E-F loop of bacteriorhodopsin. *J. Mol. Biol.* **287**: 163-171.
19. Mchaourab, H.S., T. Kalai, K. Hideg, and W.L. Hubbell, 1999, Motion of spin-labeled side chains in T4 lysozyme: Effect of side chain structure. *Biochemistry* **38**: 2947-2955.
20. Altenbach, C., T. Marti, H.G. Khorana, and W.L. Hubbell, 1990, Transmembrane protein structure: spin labeling of bacteriorhodopsin mutants. *Science* **248**: 1088-1092.
21. Farahbakhsh, Z., C. Altenbach, and W.L. Hubbell, 1992, Spin labeled cysteines as sensors for protein-lipid interaction and conformation in rhodopsin. *Photochem. Photobiol.* **56**: 1019-1033.
22. Hubbell, W.L. and C. Altenbach, 1994, Investigation of structure and dynamics in membrane proteins using site-directed spin labeling. *Curr. Opin. Struct. Biol.* **4**: 566-573.
23. Altenbach, C., D.A. Greenhalgh, H.G. Khorana, and W.L. Hubbell, 1994, A collision gradient method to determine the immersion depth of nitroxides in lipid bilayers: application to spin-labeled mutants of bacteriorhodopsin. *Proc. Natl. Acad. Sci. U S A* **91**: 1667-1671.
24. Burghaus, O., M. Rohrer, T. Gotzinger, M. Plato, and K. Möbius, 1992, A novel high-field/high-frequency EPR and ENDOR spectrometer operating at 3 mm wavelength. *Measurement Science & Technology* **3**: 765-774.
25. Prisner, T.F., A. Vanderest, R. Bittl, W. Lubitz, D. Stehlik, and K. Möbius, 1995, Time-Resolved W-Band (95 Ghz) Epr Spectroscopy of Zn-Substituted Reaction Centers of Rhodobacter Sphaeroides R-26. *Chem. Phys.* **194**: 361-370.
26. Huber, M. and J.T. Törring, 1995, High-field EPR on the primary electron donor cation radical in single crystals of heterodimer mutant reaction centers of photosynthetic bacteria - first characterization of the G-tensor. *Chem. Phys.* **194**: 379-385.
27. Stone, A.J., 1963, *Proc. Roy. Soc. London* **A271**: 424-434.
28. Plato, M., H.-J. Steinhoff, C. Wegener, J.T. Törring, A. Savitsky, and K. Möbius, 2002, Molecular orbital study of polarity and hydrogen bonding effects on the g and hyperfine tensors of site directed NO spin labeled bacteriorhodopsin. *Molecular Physics* **100**: 3711-3721.
29. Steinhoff, H.-J., A. Savitsky, C. Wegener, M. Pfeiffer, M. Plato, and K. Möbius, 2000, High-field EPR studies of the structure and conformational changes of site-directed spin labeled bacteriorhodopsin. *Biochim. Biophys. Acta* **1457**: 253-262.
30. Steinhoff, H.J., M. Pfeiffer, T. Rink, O. Burlon, M. Kurz, J. Riesle, E. Heuberger, K. Gerwert, and D. Oesterhelt, 1999, Azide reduces the hydrophobic barrier of the bacteriorhodopsin proton channel. *Biophys. J.* **76**: 2702-2710.
31. Kveder, M., A. Kriško, G. Pifat, and H.-J. Steinhoff, 2003, The study of structural accessibility of free thiol groups in human low-density lipoproteins. *Biochim. Biophys. Acta* **1631**: 239-245.

32. Griffith, O.H., P.J. Dehlinger, and S.P. Van, 1974, Shape of the hydrophobic barrier of phospholipid bilayers (Evidence for water penetration in biological membranes). *J Membrane Biol* **15**: 159-192.
33. Wegener, C., *PhD thesis*, 2002, Bochum: Ruhr-Universitaet Bochum.
34. Hustedt, E.J. and A.H. Beth, 1999, Nitroxide spin-spin interactions: applications to protein structure and dynamics. *Annu. Rev. Biophys. Biomol. Struct.* **28**: 129-153.
35. Eaton, G.R., S.S. Eaton, and L.J. Berliner, *Distance Measurements in Biological Systems*, 2000, New York: Kluwer.
36. Hustedt, E.J., A.I. Smirnov, C.F. Laub, C.E. Cobb, and A.H. Beth, 1997, Molecular distances from dipolar coupled spin-labels - the global analysis of multifrequency continuous wave electron paramagnetic resonance data. *Biophys. J.* **72**: 1861-1877.
37. Steinhoff, H.-J., O. Dombrowsky, C. Karim, and C. Schneiderhahn, 1991, Two dimensional diffusion of small molecules on protein surfaces: an EPR study of the restricted translational diffusion of protein-bound spin labels. *Eur. Biophys. J.* **20**: 293-303.
38. Rabenstein, M.D. and Y.K. Shin, 1995, Determination of the distance between two spin labels attached to a macromolecule. *Proc. Natl. Acad. Sci. USA* **92**: 8239-8243.
39. Steinhoff, H.J., N. Radzwill, W. Thevis, V. Lenz, D. Brandenburg, A. Antson, G. Dodson, and A. Wollmer, 1997, Determination of interspin distances between spin labels attached to insulin: comparison of electron paramagnetic resonance data with the X- ray structure. *Biophys. J.* **73**: 3287-3298.
40. Altenbach, C., K.J. Oh, R.J. Trabanino, K. Hideg, and W.L. Hubbell, 2001, Estimation of inter-residue distances in spin labeled proteins at physiological temperatures: experimental strategies and practical limitations. *Biochemistry* **40**: 15471-82.
41. Cai, K.W., R. Langen, W.L. Hubbell, and H.G. Khorana, 1997, Structure and Function in Rhodopsin - Topology of the C-Terminal Polypeptide Chain in Relation to the Cytoplasmic Loops. *Proc. Natl. Acad. Sci. USA* **94**: 14267-14272.
42. Altenbach, C., K. Yang, D.L. Farrens, Z.T. Farahbakhsh, H.G. Khorana, and W.L. Hubbell, 1996, Structural features and light-dependent changes in the cytoplasmic interhelical E-F loop region of rhodopsin - a site-directed spin-labeling study. *Biochemistry* **35**: 12470-12478.
43. Voss, J., W.L. Hubbell, and H.R. Kaback, 1998, Helix Packing in the Lactose Permease Determined By Metal-Nitroxide Interaction. *Biochemistry* **37**: 211-216.
44. Perozo, E., D.M. Cortes, and L.G. Cuello, 1999, Structural rearrangement underlying K+-channel activation gating. *Science* **285**: 73-78.
45. Farrens, D.L., C. Altenbach, K. Yang, W.L. Hubbell, and H.G. Khorana, 1996, Requirement of rigid-body motion of transmembrane helices for light activation of rhodopsin. *Science* **274**: 768-770.
46. Tiebel, B., N. Radzwill, L.M. Aung-Hilbrich, V. Helbl, H.J. Steinhoff, and W. Hillen, 1999, Domain motions accompanying Tet repressor induction defined by changes of interspin distances at selectively labeled sites. *J. Mol. Biol.* **290**: 229-240.
47. Pannier, M., S. Veit, A. Godt, G. Jeschke, and H.W. Spiess, 2000, Dead-time free measurement of dipole-dipole interactions between electron spins. *J. Magn. Reson.* **142**: 331-340.
48. Kurshev, V.V., A.M. Raitsimring, and Y.D. Tsvetkov, 1989, Selection of dipolar interaction by the 2+1 pulse train ESE. *J. Magn. Reson.* **81**: 441-454.

49. Borbat, P.P. and J.H. Freed, 1999, Multi-quantum ESR and distance measurements. *Chem. Phys. Lett.* **313**: 145-154.
50. Jeschke, G., M. Pannier, A. Godt, and H.W. Spiess, 2000, Dipolar spectroscopy and spin alignment in electron paramagnetic resonance. *Chem. Phys. Lett.* **331**: 234-252.
51. Jung, K., J. Voss, M. He, W.L. Hubbell, and H.R. Kaback, 1995, Engineering a Metal Binding Site Within a Polytopic Membrane Protein, the Lactose Permease of Escherichia Coli. *Biochemistry* **34**: 6272-6277.
52. Leigh, J.S., 1970, ESR rigid lattice line shape in a system of two interacting spins. *J. Chem. Phys.* **52**: 2608-2612.
53. Voss, J., L. Salwinski, H.R. Kaback, and W.L. Hubbell, 1995, A method for distance determination in proteins using a designed metal ion binding site and site-directed spin labeling - evaluation with T4 lysozyme. *Proc. Natl. Acad. Sci. USA* **92**: 12295-12299.
54. Voss, J., W.L. Hubbell, and H.R. Kaback, 1995, Distance determination in proteins using designed metal ion binding sites and site-directed spin labeling - application to the lactose permease of escherichia coli. *Proc. Natl. Acad. Sci. USA* **92**: 12300-12303.
55. Farahbakhsh, Z., K. Hideg, and W.L. Hubbell, 1993, Photoactivated conformational changes in rhodopsin: a time resolved spin label study. *Science* **262**: 1416-1420.
56. Steinhoff, H.J., R. Mollaaghababa, C. Altenbach, K. Hideg, M. Krebs, H.G. Khorana, and W.L. Hubbell, 1994, Time-resolved detection of structural changes during the photocycle of spin-labeled bacteriorhodopsin. *Science* **266**: 105-107.
57. Thorgeirsson, T.E., W.Z. Xiao, L.S. Brown, R. Needleman, J.K. Lanyi, and Y.K. Shin, 1997, Transient channel-opening in bacteriorhodopsin - an EPR study. *J. Mol. Biol.* **273**: 951-957.
58. Xiao, W., L.S. Brown, R. Needleman, J.K. Lanyi, and Y.-K. Shin, 2000, Light-induced rotation of a transmembrane alpha-helix in bacteriorhodopsin. *J. Mol. Biol.* **304**: 715-721.
59. Shin, Y., C. Levinthal, F. Levinthal, and W.L. Hubbell, 1993, Colicin E1 binding to membranes: time resolved studies of spin-labeled mutants. *Science* **259**: 960-963.
60. Subramaniam, S., I. Lindahl, P. Bullough, A.R. Faruqi, J. Tittor, D. Oesterhelt, L. Brown, J. Lanyi, and R. Henderson, 1999, Protein conformational changes in the bacteriorhodopsin photocycle. *J. Mol. Biol.* **287**: 145-161.
61. Subramaniam, S. and R. Henderson, 2000, Crystallographic analysis of protein conformational changes in the bacteriorhodopsin photocycle. *Biochim. Biophys. Acta* **1460**: 157-165.
62. Rink, T., M. Pfeiffer, D. Oesterhelt, K. Gerwert, and H.J. Steinhoff, 2000, Unraveling photoexcited conformational changes of bacteriorhodopsin by time resolved electron paramagnetic resonance spectroscopy. *Biophys. J.* **78**: 1519-1530.
63. Radzwill, N., K. Gerwert, and H.-J. Steinhoff, 2001, Time-resolved detection of transient movement of helices F and G in doubly spin-labeled bacteriorhodopsin. *Biophys. J.* **80**: 2856-2866.
64. Spudich, J.L., 1998, Variations on a molecular switch - transport and sensory signalling by archaeal rhodopsins. *Mol. Microbiol.* **28**: 1051-1058.
65. Spudich, J.L., C.S. Yang, K.H. Jung, and E.N. Spudich, 2000, Retinylidene proteins: Structures and functions from archaea to humans. . *Annu. Rev. Cell Dev. Biol.* **16**: 365-392.
66. Gordeliy, V.I., J. Labahn, R. Moukhametzianov, R. Efremov, J. Granzin, R. Schlesinger, G. Büldt, T. Savopol, A.J. Scheidig, J.P. Klare, and M. Engelhard, 2002, Molecular basis of transmembrane signalling by sensory rhodopsin II-transducer complex. *Nature* **419**: 484-487.
67. Yan, B., T. Takahashi, R. Johnson, and J.L. Spudich, 1991, Identification of signaling states of a sensory receptor by modulation of lifetimes of stimulus-induced conformations: the case of sensory rhodopsin II. *Biochemistry* **30**: 10686-92.
68. Wegener, A.A., I. Chizhov, M. Engelhard, and H.J. Steinhoff, 2000, Time-resolved Detection of Transient Movement of Helix F in Spin-labelled Pharaonis Sensory Rhodopsin II. *J. Mol. Biol.* **301**: 881-891.
69. Jeschke, G., C. Wegener, M. Nietschke, H. Jung, and H.-J. Steinhoff, 2004, Inter-residual distance determination by four-pulse DEER in an integral membrane protein: the Na+/proline transporter PutP of Escherichia coli. *Biophys. J.*, in press.
70. Jung, H., R. Rübenhagen, S. Tebbe, K. Leifker, N. Tholema, M. Quick, and R. Schmid, 1998, Topology of the Na+/Proline transporter of Escherichia coli. *J. Biol. Chem.* **273**: 26400-26407.
71. Wegener, C., S. Tebbe, H.J. Steinhoff, and H.R. Jung, 2000, Spin labeling analysis of structure and dynamics of the Na+/proline transporter of Escherichia coli. *Biochemistry* **39**: 4831-4837.
72. Jeschke, G., 2002, Distance measurements in the nanometer range by pulse EPR. *Chem. Phys. Chem.* **3**: 927-932.
73. Jeschke, G., A. Koch, U. Jonas, and A. Godt, 2002, Direct conversion of EPR dipolar time evolution data to distance distributions. *J. Magn. Reson.* **155**: 72-82.
74. Quick, M., S. Stölting, and H. Jung, 1999, Role of conserved Arg40 and Arg117 in the Na+/proline transporter of Escherichia coli. *Biochemistry* **38**: 13523-13529.
75. Quick, M. and H. Jung, 1998, A conserved aspartate residue, Asp187, is important for Na+-dependent proline binding and transport by the Na+/Proline transporter of Escherichia coli. *Biochemistry* **37**: 13800-13806.